UNIVERSITY OF CALIFORNIA,
SANTA CRUZ

From dirt to diamonds: A mineralogical comparison of granular rheologies

Senior thesis by Marshall Danese
Submitted Spring 2016

Stephanie Taylor, Shalev Simon Tov
Research Advisors

Emily Brodsky
Faculty Advisor

Table of Contents

Abstract

The geologic shear zones of the Earth contain a diverse array of mineral species in pulverized, granular form. From active fault zones to slope failure planes, sheared granular flows are a component of many human hazards. Despite this, relatively little is known about granular rheology, which can resemble a solid mass at rest, or, if significantly perturbed, a gaseous fluid. Recent research has centered on the transition between these two states, or regimes, as a result of increasing shear stress, with wide applications to fault friction and earthquake nucleation. In this paper, I further characterize the rheology of granular media by exploring and quantifying the impact of grain strength and elasticity on flow dilation and compaction, both in a long-term sense and as a response to variable shear rate. To do this, I subject granular samples of different mineralogies to shear stress by means of a commercial torsional rheometer. Hard, stiff materials such as natural diamond showed dilation with increasing shear rate, as well as a large degree of compaction over time. Softer, elastic minerals showed more complicated behavior in the transitional regime, and compacted less with time. The experiment revealed convincing evidence that grain hardness and elasticity have a significant impact on long-term compaction. To the best of our knowledge, this effect has not been previously shown experimentally or suggested theoretically. A similar, but weaker relationship also exists between transitional, shear-rate dependent behaviors. I conclude that the mineralogy of shear zones will significantly affect volumetric behavior, and postulate several mechanical explanations.

1. Introduction

Granular material is inherent to numerous geologic phenomena. At geologically active contacts, such as fault zones and landslide interfaces, shear stress will grind rocks together. This pulverization of material creates considerable amounts of unconsolidated granular material that varies in size, angularity, and composition. In turn, these granular particles can alter the physics of the shear zone by influencing friction and elasticity within the interface. For instance, fluidization of granular material in subduction zones could lubricate plate boundary thrust during earthquake rupture (Melosh, 1996). Additionally, the granular composition of slide interfaces has also been shown to affect

residual strength in landslides. This is dependent on the amount and proportion of clays present (Skempton, 1985). Generating a constitutive law that describes granular behavior in shear zones is critical in gaining a full understanding of natural hazards that involve sliding interfaces.

Subjected to shear stress, granular media has been empirically defined in terms of two extremes – the quasi-static and grain-inertial regimes. These regimes are analogously related to traditional phases of matter in that each has a distinct method of momentum transfer between particles contingent on the amount of energy, or excitation, in the system (Lu et al., 2007). In the quasi-static regime, behavior can be described as "solid-like," where grains exchange momentum in brief periods of unjamming caused by small external excitations such as acoustic vibration or shearing. Force chains between grains in the quasi-static regime are long-duration and span many particles. When external excitation increases, the granular media flows more freely, analogous to a fluid. In the grain-inertial regime, force chains become shorter (Often existing as transient binary particle collisions) and are constantly being broken and re-formed (Van Der Elst et al., 2012).

1.1. Inertial Number

The inertial number is a well-established, dimensionless number that describes a granular flow. This number compares grain inertial stresses to the confining stress and is defined below (Campbell, 2006).

$$I \equiv \frac{\text{grain inertial stress}}{\text{confining stress}} \equiv \frac{\rho d \dot{\gamma}^2}{p} \tag{1}$$

where I is inertial number, ρ is grain density, d is grain diameter, $\dot{\gamma}$ is strain rate, and p is the confining pressure. In an earthquake rupture or debris flow, a granular flow moves from the quasi-static regime (Where $I \ll 1$) to the grain-inertial regime (Where $I \gg 1$). The transition between the two states occurs at intermediate inertial numbers ($I \sim 1$). At transitional inertial numbers, many factors, such as external acoustic vibration, force chain creation and buckling, as well as grain packing configurations can all affect the

behavior of the granular flow. While behavior in the quasi-static and grain-inertial regimes is well understood, a constitutive description of rheology at transitional inertial numbers remains elusive.

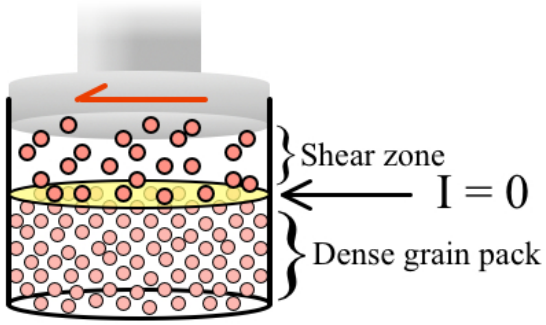

Figure 1: A diagram of a granular material subjected to shear by a rotor in a cylindrical jacket. The interface between the shear zone and the non-shearing bulk of the sample is labeled in yellow. At this interface, I = 0. Just above this interface, I > 0. The red symbol on the rotor is an indicator of shear direction. .

Because strain rate $\dot{\gamma}$ is approximately equal to shear velocity v over shear zone thickness h, equation (1) can be rearranged to predict shear zone thickness in response to change in shear velocity when inertial number I at the shear zone is ~ 1, as follows:

$$h \equiv \sqrt{\frac{\rho d v^2}{p}} \tag{2}$$

Assuming a constant confining pressure, equation (2) predicts shear zone widening as shear velocity increases, without taking into account particle elasticity or hardness. Figure 2 is a theoretical plot of this behavior, assuming the same densities as the experimental minerals (Outlined in Appendix Table A1) and a constant confining force of 1.0 N. If this equation is a complete description of volumetric dilation of a granular shear zone, experimental data should follow these predicted curves.

To get there, I will begin with a summary of previous experimentation on the subject and important background information on the types of minerals I will be using. I will then

describe the experimental setup and sample preparation, emphasizing the new aspects of the experiment. Results will show effects of mineralogy that vary with particle stiffness. A discussion follows, with analysis on both shear rate dependent change in sample thickness and long-term change in sample thickness.

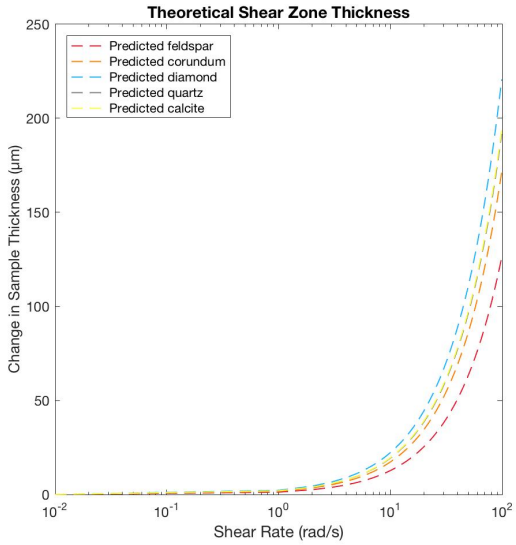

Figure 2: A theoretical plot of granular samples of different materials sheared from 10^{-3} to 100 rad/s. Equation 2 predicts a smooth increase in shear thickness, with the curve shifting left and right depending on sample density. We will add experimental data to this figure to see if equation 2 is an accurate prediction of shear zone dilation.

2. Background

2.1. Previous Experimentation

In the case of a constant pressure system, where granular shear zone thickness increases or decreases to maintain a constant confining force under increasing or decreasing shear velocities, a dip in thickness is observed at intermediate inertial numbers (Shear rate ~ 0.1-10 rad/s) (Lu et al., 2007; Van Der Elst et al., 2012). These experiments suggested that this volumetric compaction was dependent on the amount of acoustic vibration produced internally. When acoustic vibration is measured, it is observed that a period of high acoustic noise beginning at shear rates around 0.1 rad/s coincides with the change in rheology.

Acoustic noise was significantly influenced by grain angularity. While highly angular quartz beach sand generated sufficient acoustic noise and showed this auto-acoustic dip, spherical glass beads did not (Van Der Elst et al., 2012). When acoustic pulses were externally applied to the system resulted in shear zone compaction at lower velocities. These observations indicate that change in shear zone thickness is likely a function of the competition between confining pressure and internally generated acoustic pressure. Change in the magnitude of either confining pressure or acoustic vibration with respect to the other can result in this anomalous rheological behavior in certain conditions (Van Der Elst et al., 2012). This transitional phase at intermediate inertial numbers was named the auto-acoustic regime.

These experiments were followed by a study with a similar setup, in which the effect of median grain diameter was assessed. By separating grains into bins of varying sizes, it was observed that between inertial numbers of 10^{-4} and 10^{-2}, granular material below approximately 250 μm in diameter showed a similar amount of compaction, while material above that threshold did not. When the grain size distribution spanned both small and large grain diameters, the compaction took on the behavior of the smallest grain sizes. It was concluded that while smaller grains produced more noise at lower inertial numbers, compaction was not directly related to the magnitude of acoustic noise produced (Taylor and Brodsky, 2013).

Looking beyond particle size and angularity, mineralogy and composition of the granular media also has potential for influencing the behavior of the flow.

2.2. Mineralogy in Shear Zones

Granular material found within shear zones in nature, such as fault gouge or the clay layer of a landslide slide plane, sometimes have the same mineralogy as their parent rocks, but they often vary considerably due to physical or chemical alteration. Because of the differential permeability between granular material versus an unfractured, solid mass, comminuted material in shear zones are differentially susceptible to chemical alterations when compared with their parent rock. Infiltrating water can alter the composition of a shear zone by dissolving, oxidizing, or otherwise reacting with the material, as well as by introducing foreign solutes (Fetter, 2001).

While fault gouge typically consists of common minerals such as quartz and feldspar, more infrequently occurring minerals such as ferromagnesian silicates (E.g., biotite), iron oxides (E.g., magnetite, maghmeite), and carbonates (E.g., siderite, calcite) are also observed. Chemically decomposed minerals are present in fault zones as clays, such as kaolinite, chlorite, and fine muscovite, among others (Caine & Bove, 2010). In addition to chemical alteration, granular media within fault zones are susceptible to mineralogical changes as a result of extreme environmental stress and metamorphism (Kameda et al., 2011). Moreover, these mineralogical changes can have profound effects on shear zone mechanics. For example, decarbonation ($CaCO3 \rightarrow CaO + CO2$) in fault zones decomposes carbonate into Calcium oxide (A.k.a. 'quicklime,' or 'burnt lime'), but also decreases shear zone slip-resistance by increasing pore fluid pressure and temperature (Sulem and Famin, 2009). Understanding granular rheology within the scope of variable mineralogy could give us further insight into earthquake nucleation and propagation in nature.

The physical properties of individual grains, including strength, density, fracture toughness, and elastic modulus, all have the potential to impact the rheology of a flow. For example, a weaker grain could create acoustic vibration of a greater magnitude than a stronger grain. A material's elasticity also has potential to affect stick-slip behavior, which could also affect compaction and dilation over shear rates. I predict that where strong, elastic grains will rub and roll over each other when shear force is applied, more weak and brittle grains might simply fracture. Fracturing material implies greater long-term compaction due to increasing packing density from smaller grains filling in void space, and possibly greater volumetric compaction during the auto-acoustic phase due to more vibration. Alternatively, stiffer minerals could produce greater inertial rebound forces between grains, compacting the sample more over time.

3. Experimental Setup & Procedure

To further expand on the characterization of the transitional rheological regime, I measured the influence of grain mineralogy on granular rheology under shear stress. Using a similar experimental setup to previous experiments, I investigated minerals with widespread geophysical applicability and variable intrinsic physical properties.

Ultimately, I measured the influence of specific physical properties on the presence of an auto-acoustic regime.

I chose diamond, corundum, garnet, quartz, potassium feldspar, apatite, and calcite as initial foci for experimentation. These minerals encompass a wide range of hardness and elasticity. A table of researched and experimentally derived mineral properties is located in the appendix.

The experimental apparatus is similar to the one used in *Lu et al [2007]* and *van der Elst et al [2012]*. The TA Instruments AR2000ex commercial torsional rheometer has a rotating parallel plate geometry that has been modified slightly for use with non-fluid samples. A schematic of the setup is provided in figure 1. The rheometer measures torque within a 1 nN-m tolerance, absolute sample height within a 1 μm tolerance, normal force within a 1 mN tolerance, and angular velocity within a range of 10^{-3} and 300 rad/s. The experiments are conducted with a 1 Hz sample rate at 25ºC in a climate-controlled lab.

The granular sample is housed in a 19 mm diameter quartz jacket carefully affixed to the base of the rheometer using a centering device (Further described in § 2). This ensures minimum residual torque, between 10 to 50 μN-m, or less than 0.01% of the average torque observed during shearing. The base plate also houses the force transducer and Peltier Plate temperature control. Grains of the sample material are epoxied to the 19 mm top rotating plate and super-glued to the base of the jacket to generate internal shear rather than boundary slip. The quartz cylinder is 15 mm in height, but the sample is only filled to about 8 to 10 mm such that the top plate is partially jacketed.

All experiments are carried out under controlled normal pressure conditions. This is maintained by adjustment of sample thickness, through a slow feedback that will only respond if a fluctuation in normal pressure exceeds 10% of the target 3.527 kPa value (1 N normal force over the sample area). This results in sample thickness fluctuations in response to sudden changes in normal pressure that can be seen as a hysteresis in sample thickness between opposite-direction velocity ramps. This drawback of the experimental setup is further described in the discussion §4.

3.1. Sample Acquisition and Preparation

Samples were chosen, prepared and analyzed in a variety of ways. Minerals were selected to span a wide range of Moh's hardnesses, from 4 (Calcite) to 10 (Diamond).

While diamond, corundum, and quartz were available in granular form, samples of garnet, potassium feldspar, apatite, and calcite were obtained as whole crystals and processed with a Spex 8510 Shatter Box and/or a motor and pestle to achieve the desired grain size. All samples were sieved to 180-250 μm in diameter. Grain angularity was not measured. This grain size was chosen because it shows the greatest acoustic noise and compaction during the transitional regime (Taylor and Brodsky, 2013).

We purchased 177 μm natural diamond grains from Eastwind Diamond Abrasives and 220 μm corundum grains from Panadyne, Inc. 180-250 μm quartz-based beach sand was acquired from Natural Bridges State Beach in Santa Cruz, California. Garnet, potassium feldspar, apatite and calcite samples were donated by the UC Santa Cruz mineral collection.

3.2. Procedure

To set up the experiment, between three and four grams of sample are placed in the glass jacket. The rotor is carefully centered such that the residual torque is between 10 and 50 μN-m, and grains of matching mineralogy are epoxied to the top plate and left to dry for 24 hours. The rotor is rotationally mapped to further minimize residual torque.

The procedure consists of multiple continuous velocity ramps to condition the material, followed by peak hold steps that mimic the stepped-flow steps in *van der Elst [2012]* and *Taylor & Brodsky [2013]*. Peak hold steps were chosen over the previously employed stepped-flow steps in order to sample at a higher 1 Hz rate. An ideal experiment consists of 2-8 conditioning continuous velocity ramps, followed by 5 to 13 'runs.' Each run consisted of 51 peak hold steps that logarithmically increased or decreased in shear rate from 10^{-3} to 100 rad/s. These steps are further detailed in §s 2.3.1 and 2.3.2, below. Both continuous ramp steps and peak hold runs alternated between increasing and decreasing shear rate.

3.2.1. Continuous Velocity Ramps

Each experiment had four continuous ramp steps. These steps continuously move through shear velocities over a user-specified period (In our case, 10 minutes). The

objective was to condition the material into a more stable compaction. Ideally, by the end of the four continuous ramp steps, the sample behavior is repeatable and shows minimal hysteresis between steps with increasing shear rate, or "up ramps," and steps with decreasing shear rate, or "down ramps." After four continuous ramp steps, the peak hold phase of the experiment was initiated.

3.2.2. Peak Hold Steps

After the sample is conditioned, we begin a series of 'peak hold' steps, in which one velocity is held for a set period of time. Each of the five decades has 10 peak hold steps shearing at a logarithmically increasing rate between 10^{-3} and 100 rad/s. Unlike the continuous velocity ramp, peak hold steps hold the shear constant for a set amount of time. In these experiments, each peak hold step is held for 40 seconds to allow the flow to reach steady state (Described more in Figure 3). Each 'run,' or series of 51 peak hold steps of increasing shear rate, lasts 34 minutes. For visual aide, Figure 4 divides an experiment into runs.

In all experiments, one data point per second is recorded. This contrasts to the previously used 'stepped flow' procedure in *van der Elst [2012]* and *Taylor & Brodsky [2013]*, where the shear rate is successively increased every 40 seconds, and only the mean of the last 20 seconds of a velocity step is recorded. In this paper, averaging similar to this was done in post-experiment analysis in MATLAB. Other than sampling rate, the experiment is identical.

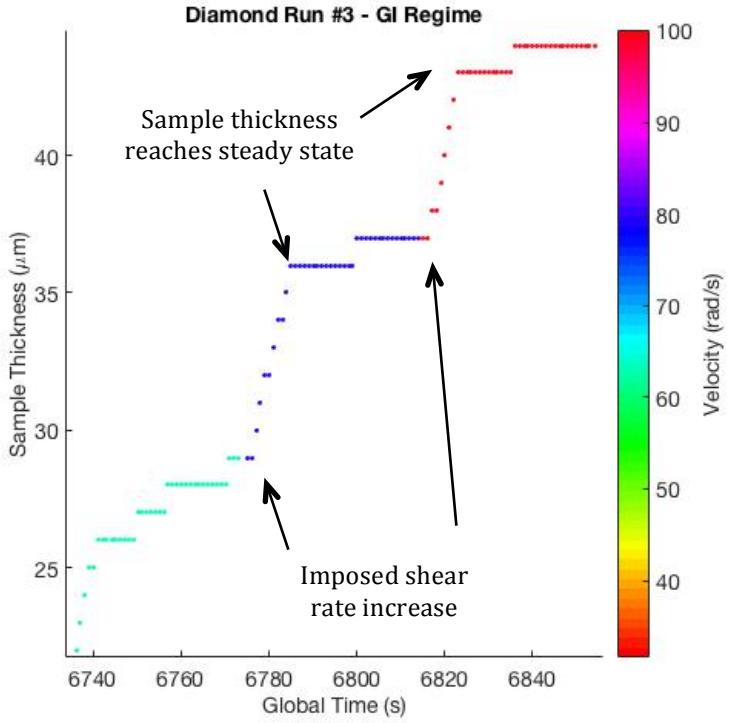

Figure 3: Plot of sample thickness versus global time, with peak hold step velocity indicated by color. This is a representative portion of a diamond experiment in the grain-inertial regime, used to illustrate the sample achieving steady state in the last 20 to 30 seconds of each peak hold step. When the rotor imposes a new shear rate, the sample thickness increases rapidly in the first 10-20 seconds, before leveling off and remaining relatively stable.

4. Results

Two forms of sample thickness change were evident in the data. When sample thickness (normalized to grain diameter) is compared with the total time of the experiment (See Figure 5), long term, or 'slow' compaction differs in magnitude between mineralogies. The other form of compaction was dependent on shear rate. The shape of the shear-rate dependent compaction is discussed in terms of the presence, magnitude and position of the compaction in intermediate inertial numbers as well as the stability and nature of the quasi-static and grain-inertial regimes. Note that if multiple mineralogies are present on a single plot, diamond is always denoted blue, corundum orange, garnet

purple, quartz black, feldspar red, apatite green, and calcite yellow. Change in sample thickness will be shown as a fraction of *initial* grain diameter.

4.1. Long-Term Compaction

The rate of long-term compaction was independent of shear rate and decreased with time, although it never fully reached zero. Run 5 was chosen as a point of LTC comparison because it is the furthest run that has data from all minerals. By the beginning of run five, diamond showed the most long-term compaction of about 0.58 of initial grain diameter, and feldspar showed the least at 0.12 grain diameters. All of these values are enumerated in Table 1. Likely, this compaction is happening in the non-shearing bulk of the sample, for reasons discussed later (Chambon et al., 2006).

Mineral Name	**Long-Term Compaction at Run 5** (As a fraction of grain diameter)
Diamond	0.58
Corundum	0.49
Quartz	0.20
Feldspar	0.12
Calcite	0.16

Table 1: Total long-term compaction was calculated from the minimum value of run four, compared with the minimum value of run one. Run four was chosen because this is the latest run with all mineral data available.

Fitting a quadratic trend line to each experiment shows decreasing rate of compaction with time for all minerals but calcite. The greatest amount of compaction occurs after a high velocity peak, when the rotor is decreasing in velocity. In hard, inelastic minerals like diamond, the amount of sample compaction that takes place after a velocity peak is over two times the amount of dilation that takes place when shear rate is increasing. Allowing the rotor to maintain a peak hold at a high velocity for five minutes during the conditioning phase did not significantly affect the rate of compaction over time, although grain crushing at these high velocity peak holds in weaker materials did lead to some compaction.

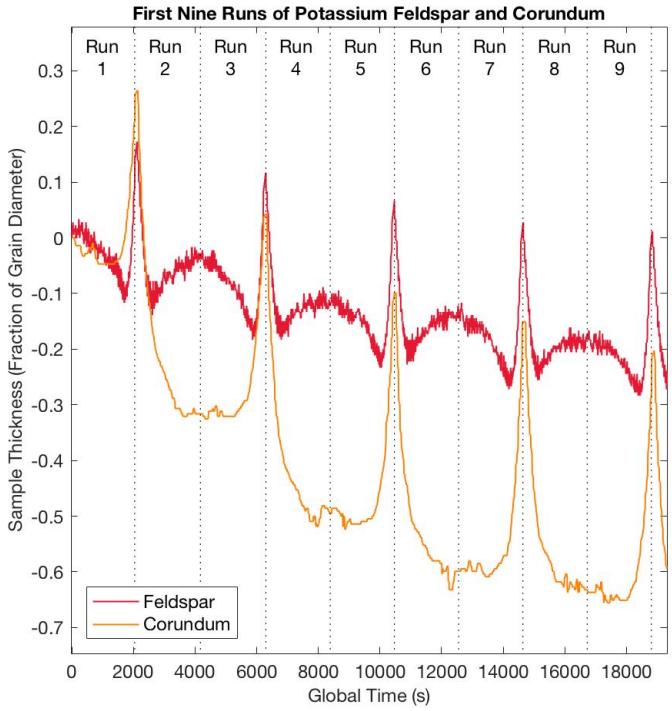

Figure 4: Plot of sample thickness versus global time. For simplicity, only potassium feldspar and corundum are shown in this graph. All experiments are plotted in Figure 5. Dotted lines are added to help visualize what we define as a 'run'. Additionally, note the difference in compaction rate with time and magnitude of shear zone thickening between the two minerals.

4.2. Shear Rate Dependent Compaction

Shear rate dependent compaction can be measured by the presence, size, and position of the auto-acoustic dip with respect to inertial number, as well as the total change in sample thickness over a run (Sample thickness at 10^{-3} rad/s and 100 rad/s). The hysteresis between up ramps and down ramps discussed in §2 is visible in Figure 7. When inspecting the residual plot, runs with decreasing shear rate show a lesser degree of auto-acoustic compaction in general, and this is true for all mineralogies. As discussed in §2, this likely has to do with the normal force control software.

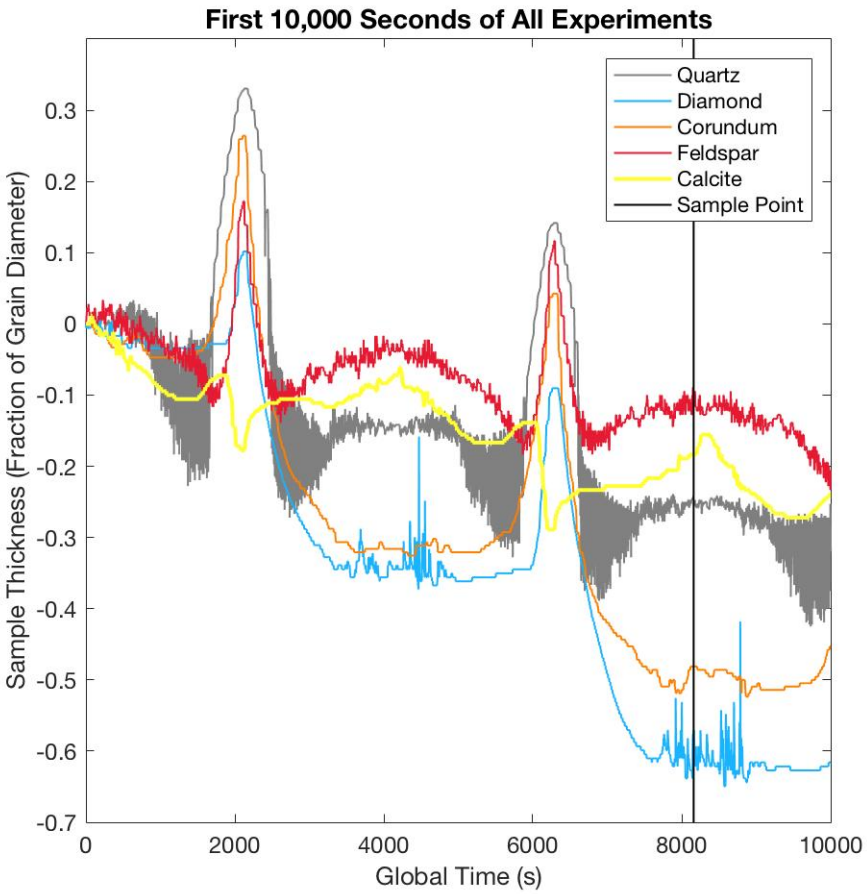

Figure 5: Similar to Figure 4, but with all minerals over the first 10,000 seconds. Slope of long-term compaction over time is usually higher for harder minerals. One exception to this is calcite, which shows greater compaction over time than feldspar. While softer, calcite is a more inelastic mineral. Long term compaction is measured from initial thickness to the sample point, at 8160 seconds. This is the beginning of the fifth run for each experiment, the importance of which is discussed in § 4.1.

In all other cases, I forego fitting the data to a trend line to correct for long-term compaction, and directly compare sample thickness (Again, as a fraction of grain size), to inertial number. Overall, stronger minerals such as diamond and corundum had the greatest increase in thickness in the grain-inertial regime. Per run, corundum had the greatest average change (0.328 grain diameters), while calcite had the smallest (0.168 grain diameters) (All results in Table 2).

Mineral Name	**Average change in thickness** (As a fraction of grain diameter)
Diamond	0.328
Corundum	0.380
Quartz	0.320
Feldspar	0.176
Calcite	0.168

Table 2: Average change in thickness is calculated by the absolute value of the difference between grain-size-normalized sample thickness at the first peak hold step and the last peak hold step, averaged over runs.

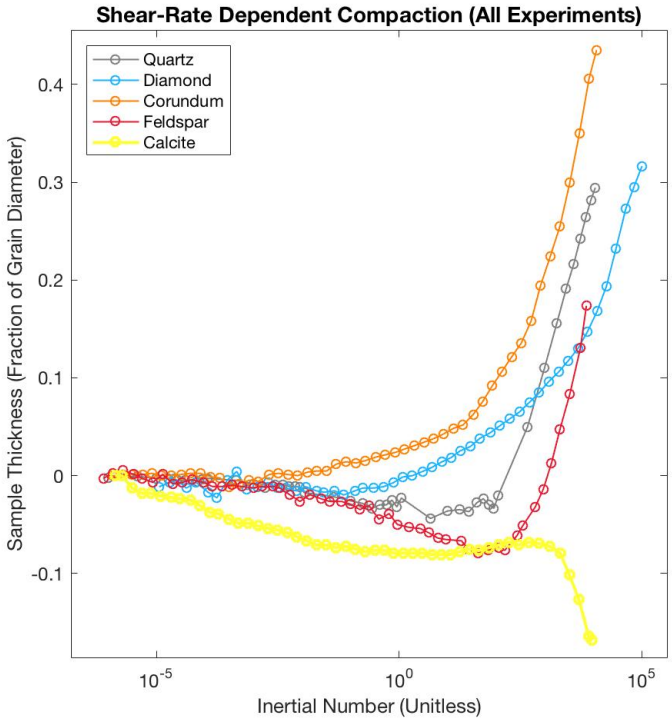

Figure 6: Plot depicts sample thickness as a fraction of grain diameter by inertial number. Peak hold steps are averaged to the last 20 seconds, and once again averaged between all runs. Auto-acoustic dip is evident in both quartz and feldspar, as well as in preliminary experiments on garnet (Not plotted).

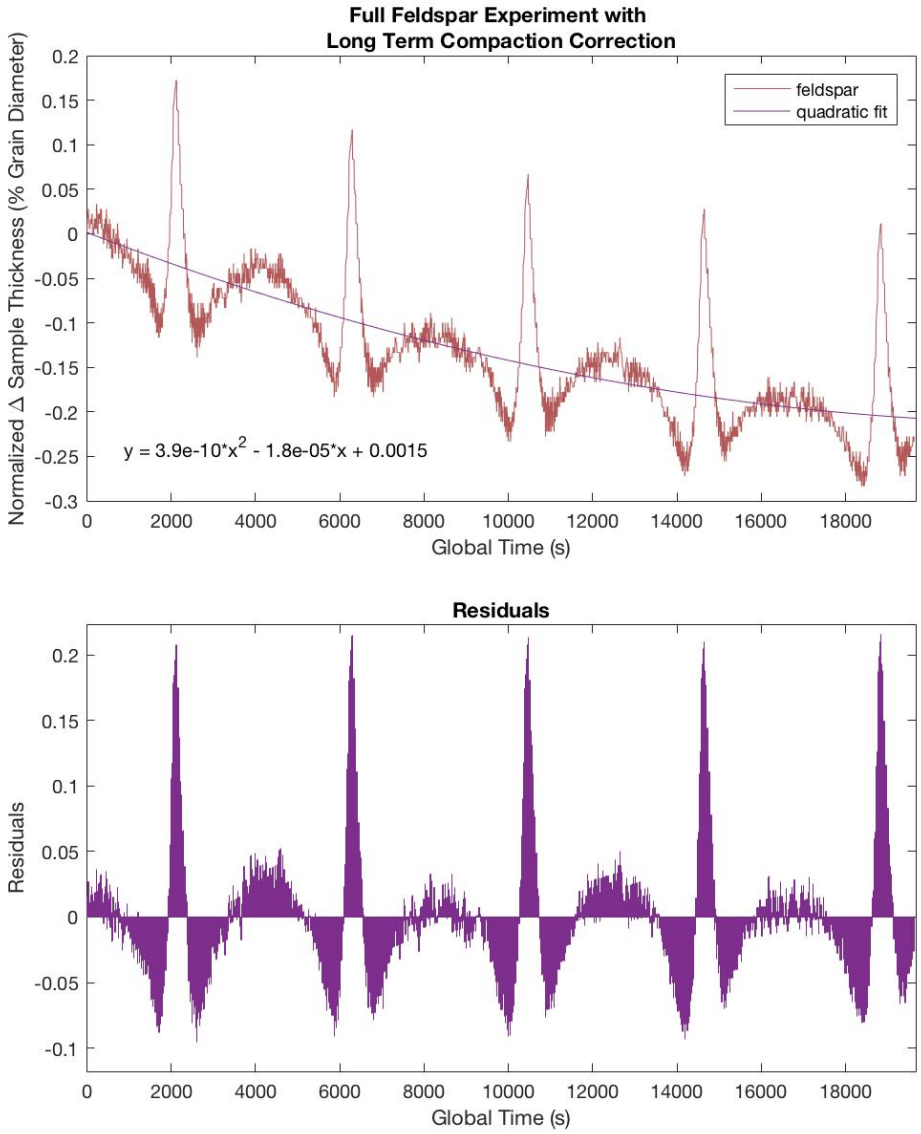

Figure 7: Change in sample thickness as a fraction of grain diameter for feldspar experiment by global time (Above), and the residuals of a quadratic fit line (Below). This method can be used to correct for compaction over time. Hysteresis between runs that increase in shear rate versus runs that decrease in shear rate is still evident when viewing the residual graph. Auto-acoustic compaction is smaller in magnitude in runs with decreasing shear rate. This is typical of all minerals that showed compaction during the transitional regime.

5. Discussion

In this section, I interpret the results by comparing experimentally observed changes in shear zone thickness to the predictions of equations 1 and 2. I will further define the effect of mineralogy on our results by describing how the samples behaved over multiple shear cycles, and also by looking at each sample's thickness curve shape and size in terms of mineral properties.

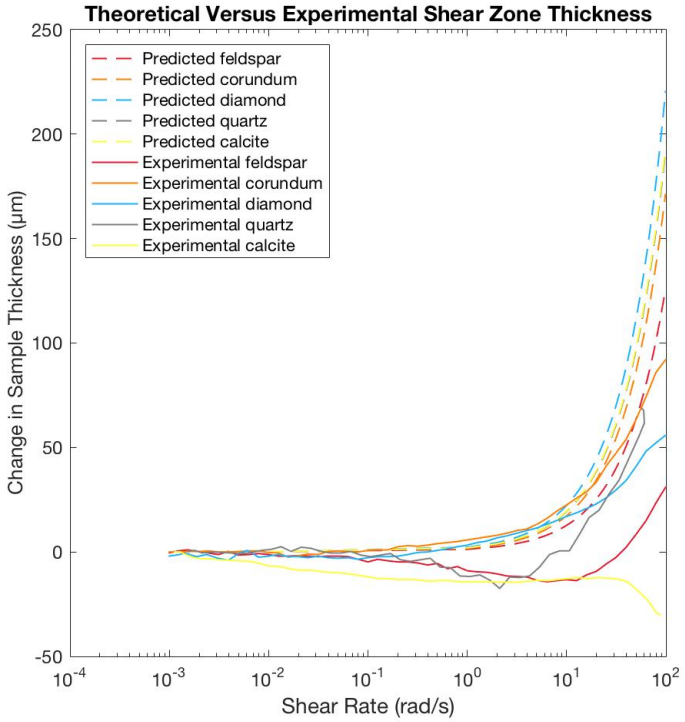

Figure 8: Plot shows both theoretical and experimental shear zone thickness. Equation (2) fails to take into account several important factors in shear zone dilation and compaction.

When experimental data is added to Figure 2, the theoretical plot of feldspar and corundum, it is clear that a part of the picture is missing (Figure 8). While the basic trend of higher density materials expanding at lower velocities holds true, a ~ 80 μm portion of dilation in both feldspar and corundum remains unaccounted for. On top of this, the shape of feldspar's change in thickness varies significantly from the simple exponential curve given by equation (2), whereas the shape of corundum's change in thickness remains

similar. Equation (2) seems to accurately predict the thickness of hard, inelastic grains at most velocities, but falls apart when sample material is soft and elastic.

5.1. Effect of Mineralogy on Long-Term Compaction

To begin to understand how the physical properties of individual grains affect rheology, we inspect a plot of many shearing cycles. Comparing the compaction over five runs with mineral properties reveals a striking relationship between material elasticity and long-term compaction (Depicted in Figure 9). Using Spearman's rank-sum test for correlation, the relationship is significant with a p-value of 0.01667.

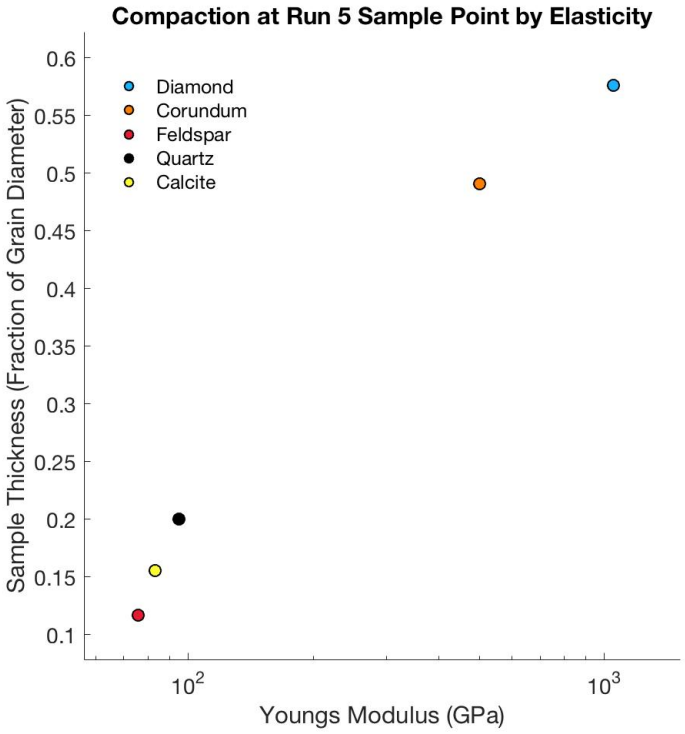

Figure 9: This plots compares Young's modulus with a measure of long-term change in sample thickness (Measured from the initial thickness to the thickness at the first step of run five, as indicated on Figure 5). Elasticity is highly correlated with the magnitude of long-term compaction.

It is suggested that the interfacial layer of grains is not involved in long-term compaction, and instead this compaction is from the bulk of the sample (Chambon et al.,

2006). These data, while initially counterintuitive, can be justified theoretically. As grain stiffness increases, force chains should become more resistant to buckling and thus the sample should not compact as much over time. Yet, these results show the opposite trend, and quite convincingly. Complimentary to compacting more as shear rate decrease, stiffer minerals tend to dilate more as shear rate increases (Figure 4 illustrates this well) In higher stiffness systems, the rebound force from impacting grains causes this higher magnitude of dilation (Andreotti 2013). As shear rate decreases, the opposite is likely true, and the inertia of a stiff granular system could allow for exploration of denser packing configurations and greater compaction.

5.2. Effect of Mineralogy on the Auto-Acoustic Regime

In addition to compaction over many shear cycles, there are several weaker lines of evidence that point to a correlation between grain hardness and elasticity and the magnitude of the auto-acoustic dip at intermediate inertial numbers. Additionally, a similar relationship exists between these properties and the position of maximum compaction, relative to inertial number.

Average total compaction is used a proxy for auto-acoustic dip magnitude. Average total compaction was measured by calculating the difference between the initial sample thickness and the minimum sample thickness. Vicker's hardness and Young's modulus were not well correlated with average total compaction, although a trend existed. It appears that, as a mineral becomes harder, the magnitude of compaction during the auto-acoustic regime decreases. In the case of diamond and corundum (Figure 10), total compaction was around 1 μm, which is close enough to zero to be considered noise in the experiment.

(a)

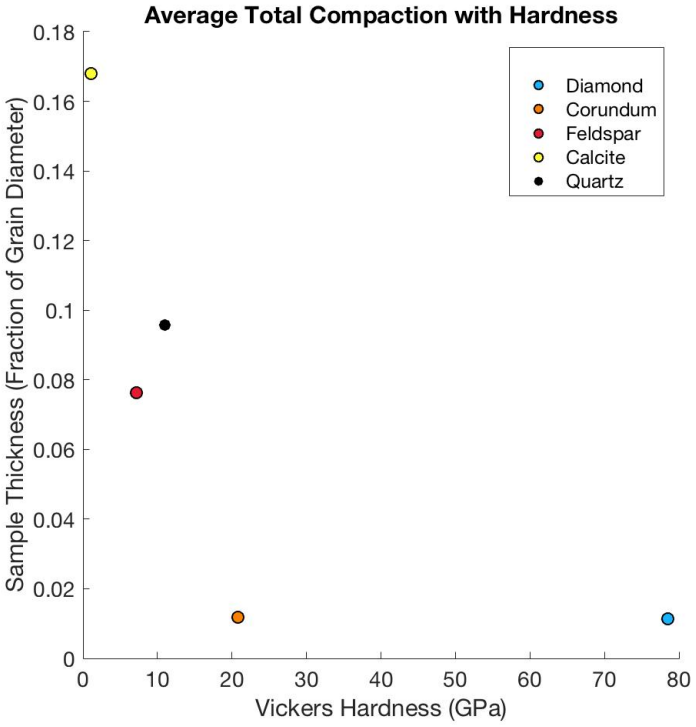

(b)

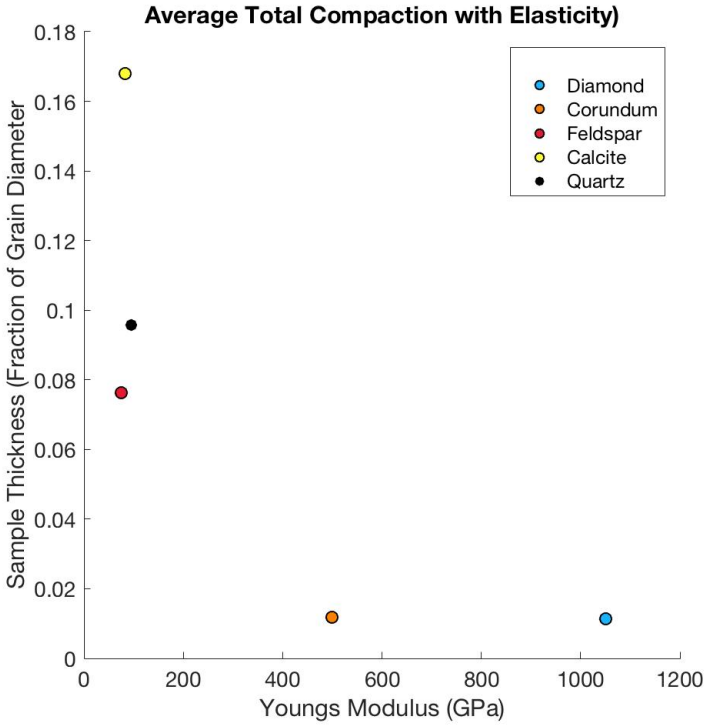

Figure 10: These plots compare (a) Vickers hardness and (b) Young's modulus with the average total compaction of each mineral. Hardness and elasticity were both negatively correlated with average compaction.

Moving on, I sought to assess how these properties affected the position of auto-acoustic dip with respect to inertial number. To do this, I compared each mineral's Vickers hardness and Young's modulus with the inertial number at which the sample reached minimum thickness. This told a similar story. The inertial number at which maximum compaction occurred, on average, was correlated loosely with the Vickers hardness and Young's modulus of each mineral in a similar way to the magnitude of average total compaction. In other words, the inertial number at which the auto-acoustic dip occurs is correlated with material properties in a similar way to dip magnitude. A weaker, more elastic material is more likely to have a larger auto-acoustic dip that occurs at a lower inertial number when compared to a strong, inelastic material.

5.4 Sources of Error and Caveats

The unresponsive normal force feedback algorithm was likely the sole cause of the compaction hysteresis seen between runs (See figure 7). I was unable to correct for this flaw, and it leads to a significant trend in the results. Additionally, while research on the subject is limited, compaction is likely more efficient when applying vibration in cyclic bursts that allow the media to settle between cycles (Andreotti, 2013). This could have some positive affect on the magnitude of compaction while shear rate was decreasing, and the upper plate cyclically clamped down on the sample and lifted up to overcorrect.

Comminution of the softer minerals could have affected total long-term compaction measurements, because small, fractured grains will more readily fill in void space. This increases packing density, which will increase the magnitude of compaction. Because the rate of crushing with time was not assessed, this issue was not corrected for. A larger issue was the apparent powderization of calcite. Calcite in the interfacial layer decreased an estimated 100 μm in diameter, on average. This allowed the powder to enter the microns-wide gap between the upper rotor plate and the quartz jacket. I could not measure total mass escaped from the system, so it was not corrected for. Additionally, a significant amount of the compaction is likely due to comminution of grains, especially at higher inertial numbers ($>10^3$).

Caution should be exercised when drawing conclusions from the position of the auto-acoustic regime with respect to inertial number in harder minerals such as diamond and corundum, because average total compaction was small enough to simply be noise in sample thickness.

6. Conclusion

Mineral properties do exert some control over granular rheology. Most convincingly, the Young's modulus of the material is strongly correlated with the magnitude of compaction over several shearing cycles. Vickers hardness has a similar relationship with long term compaction, although the correlation is weaker. It is more difficult to directly link shear rate dependent compaction mineralogy, although a trend exists. Soft, elastic

minerals showed a greater dip at intermediate inertial numbers, similar to the observations made by *Lu et al 2017* and *van der Elst et al 2012*, but this trend broke down once the grains began to fracture and eventually powderize. Some drawbacks to our methods exist, however. Primarily, the slow feedback from the normal force control software affected our ability to constantly shear the material, and led to oscillations in normal pressure.

Going further, experiments should assess how acoustic amplitude is affected by mineralogy. Unfortunately, without this information, a significant portion of the picture is missing. It is unclear whether harder minerals do not show compaction at intermediate velocities due to lower-magnitudes of internal vibrations, or if the dilation of stiff granular material simply overpowers the auto-acoustic compaction observed in weaker material.

Appendix

Mineral Name	Vicker's Hardness (GPa)	Young's Modulus (GPa)	Density (g/cm^3)
Diamond	78.5[1]	1050[2]	3.51[1]
Corundum	20.85[4]	400[1]	4.02[1]
Garnet	15.1[1]	300	3.93[1]
Quartz	11.03[4]	95[1]	2.65[1]
Feldspar	7.14[4]	75.58[5]	2.56[1]
Calcite	1.05[4]	83[1]	2.7102[6]

Table A1: Vickers hardnesses and young's moduli were researched for each mineral. Sources are as follows: 1) (Weber, 2003); 2) (Klein and Cardinale, 1993); 4) (Taylor, 1949); 5)(Taylor, 1949) (Ramirez) 6) Mindat.org

References Cited

Bruno Andreotti, 2013, Granular Media: Between Fluid and Solid. http://www.edition-sciences.com/milieux-granulaires-entre-fluide-et-solide.htm

Campbell, C.S., 2006, Granular material flows – An overview: Powder Technology, v. 162, no. 3, p. 208–229, doi: 10.1016/j.powtec.2005.12.008.

Chambon, G., Schmittbuhl, J., and Corfdir, A., 2006, Frictional response of a thick gouge sample: 1 mechanical measurements and microstructures: Journal of Geophysical Research: Solid Earth, v. 111, no. 9, p. 1–17, doi: 10.1029/2003JB002731.

Van Der Elst, N.J., Brodsky, E.E., Le Bas, P.Y., and Johnson, P. a., 2012, Auto-acoustic compaction in steady shear flows: Experimental evidence for suppression of shear dilatancy by internal acoustic vibration: Journal of Geophysical Research: Solid Earth, v. 117, no. 9, p. 1–18, doi: 10.1029/2011JB008897.

Fetter, C.W., 2001, Applied Hydrogeology:.

S.C., Jonathan, Dana J. Bove, U., 2010, Rock Geochemistry and Mineralogy from Fault Zones and Polymetallic Fault Veins of the Central Front Range , Colorado Data Series 492: Data Series, v. 492, p. 6.

Kameda, J., Ujiie, K., Yamaguchi, A., and Kimura, G., 2011, Smectite to chlorite conversion by frictional heating along a subduction thrust: Earth and Planetary Science Letters, v. 305, no. 1-2, p. 161–170, doi: 10.1016/j.epsl.2011.02.051.

Klein, C.A., and Cardinale, G.F., 1993, Young’s modulus and Poisson's ratio of CVD diamond: Diamond and Related Materials, v. 2, no. 5-7, p. 918–923, doi: 10.1016/0925-9635(93)90250-6.

Lu, K., Brodsky, E.E., and Kavehpour, H.P., 2007, Shear-weakening of the transitional regime for granular flow: Journal of Fluid Mechanics, v. 587, p. 347–372, doi: 10.1017/S0022112007007331.

Melosh, H.J., 1996, Dynamic weaking of faults by acoustic fluidization: Nature, v. 379, p. 601, doi: 10.1038/379601a0.

Ramirez, J. Microindentation and Fracture of Mineral Rock. Nanovea, Inc., 2010.

Skempton, A. W., 1985, Residual strength of clays in landslides, folded strata and the laboratory*: Géotechnique, v. 35, no. 1, p. 3–18, doi: 10.1680/geot.1985.35.1.3.

Sulem, J., and Famin, V., 2009, Thermal decomposition of carbonates in fault zones: Slip-weakening and temperature-limiting effects: Journal of Geophysical Research, v. 114, no. B3, p. B03309, doi: 10.1029/2008JB006004.

Taylor, E.W., 1949, Correlation of the Mohs's Scale of Hardness with the Vickers's Hardness Numbers: Mineralogical Magazine, v. 28, p. 718–721, doi: 10.1180/minmag.1949.28.206.08.

Taylor, S., and Brodsky, E.E., 2013, Grain size distributions and their effects on auto-acoustic compaction: American Geophysical Union,. Fall meeting abstract # EP13C-04

Weber, Marvin J. *Handbook of Optical Materials*. Boca Raton: CRC, 2003. Print.